Modelling hyperfine interactions for nuclear g-factor measurements

B.P. Mccormick, A.E. Stuchbery, A. Goasduff, A. Kusoglu, G. Georgiev

Modelling hyperfine interactions for nuclear g-factor measurements

B. P. McCormick[1,*], A. E. Stuchbery[1,**], A. Goasduff[2], A. Kusoglu[2,3], and G. Georgiev[1,2]

[1]Department of Nuclear Physics, Research School of Physics, The Australian National University, ACT 2601, Australia
[2]CSNSM, CNRS/IN2P3, Université Paris-Sud, UMR8609, F-91405 ORSAY-Campus, France
[3]Department of Physics, Faculty of Science, Istanbul University, Vezneciler/Fatih, 34134, Istanbul, Turkey

Abstract. A promising technique for g-factor measurements on short-lived nuclear states utilises the hyperfine fields of free ions in vacuum. To fully utilise this technique the hyperfine interaction must be modelled based on atomic structure calculations. Atomic structure calculations were performed using the most recent release of the General Relativistic Atomic Structure Package, and Monte-Carlo simulations of atomic-decay cascades in highly charged ions were developed. The simulations were used to fit experimental data on excited ^{56}Fe ions recoiling in vacuum with a view to determining the first-excited state g factor, $g(2_1^+)$, of ^{56}Fe.

1 Introduction

A powerful probe for nuclear structure study is the magnetic dipole moment, μ. Usually, for excited states, the g factor is the quantity measured, where $g = \mu/I$, I being the spin of the state. The g factor provides a way to probe the wavefunction of a single state. It is sensitive to the composition of broken proton vs neutron pairs, and the angular momentum they carry. Often, these states have lifetimes in the picosecond range, requiring kilotesla-strength fields to perform g-factor measurements. Such fields can only result from hyperfine interactions. Two useful hyperfine fields are the transient field [1], resulting from the interaction between a ferromagnetic solid and a swift ion traversing it, and the hyperfine field produced by the electron cloud surrounding the nucleus of a free ion [2]. In the late 1960s, Goldring *et al.* characterised the hyperfine interactions of ions that had recoiled into vacuum or low-density gas at velocities of a few percent of the speed of light [3]. The hyperfine interaction, which depends on the g factor, perturbs the distribution of γ-rays from the nuclei. Thus, the g factor can be determined. After the transient field effect was discovered, however, it became the primarily used method to measure the g factors of short-lived states, from the mid-1970s onward.

The hyperfine field method was largely neglected until 2005 when Stone *et al.* used the recoil-in-vacuum (RIV) technique to measure $g(2_1^+;^{132}\text{Te})$ using a radioactive ion beam (RIB) [4]. The RIV technique allows the unreacted radioactive beam to travel out of view of the γ-ray detectors, avoiding the accumulation of background radiation (a major problem for transient-field measurements [4]). Additionally, modern detector arrays allow for the coverage of a large solid angle. ^{132}Te $g(2_1^+)$ was determined by calibrating the hyperfine interaction with the known g factors and lifetimes of even-even stable Te isotopes. The success of this approach led to several RIB RIV measurements on nearby nuclides [5–7]. In principle, it should be possible to determine g factors based on calculated hyperfine-field strengths. By performing a time-dependent (TD) RIV measurement, the nuclear precession frequency resulting from a simple hyperfine interaction can be measured directly. This technique was applied in the measurement of $g(2_1^+;^{24}\text{Mg})$ [8], which produced a precise value due to the small systematic uncertainty. One advantage of this particular method is that bare and H-like charge states were dominant, making for a straight-forward analysis of the results. However, as higher-Z nuclei are considered, the H-like interaction becomes too high in frequency to resolve its time dependence. To reduce the hyperfine-field strength into the regime where its frequency can again be resolved requires measurements on multi-electron ions. The challenge to calculate the relevant hyperfine interactions then becomes more complex. Measurements on some multi-electron systems neighbouring each other have produced results that are difficult to interpret [2], but imply that a few low-excitation atomic configurations must be dominant. To tackle the challenge of identifying these important atomic configurations, we model the hyperfine interaction by performing atomic structure calculations and evaluating the effect of atomic transitions in an ensemble of ionic states by the Monte Carlo method [9, 10].

The Monte-Carlo method is performed by populating a large number of atomic states across the relevant charge-state distribution and simulating their decays. The contribution of each individual decay path is then averaged. A similar approach has been applied by Chen *et al.* [11], but it was not applied to time-dependent measurements. It also did not allow the initial distribution of atomic states

*e-mail: u5600477@anu.edu.au
**e-mail: andrew.stuchbery@anu.edu.au

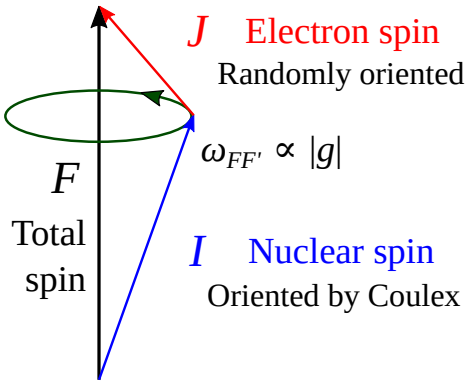

Figure 1. Spin coupling between the nuclear (I) and electron (J) spins, combining such that $F = I + J$. The dipole interaction results in a precession about F with angular frequency $\omega_{FF'}$ [see Eq. (2)].

to be parametrized. In this work, a modified approach is presented for the analysis of TDRIV data. Data taken on the ^{56}Fe 2_1^+ state are used to demonstrate the analysis, and a tentative value for $g(2_1^+;^{56}\mathrm{Fe})$ is deduced.

2 Methods

2.1 The ^{56}Fe time-differential recoil-in-vacuum measurement

A TDRIV experiment was conducted at the ALTO facility at the IPN, Orsay, in which a 130 MeV ^{56}Fe beam was incident upon a target having 230 μg/cm^2 of carbon on a 0.5-μm-thick nickel foil. Beam particles were excited on the carbon layer and recoiled out of the nickel. The OUPS plunger device [12] was used to detect forward-scattered carbon ions, and recoiling beam particles were stopped in a thick nickel foil (5.8 mg/cm^2). The OUPS is capable of adjusting the foil position along the beam axis in order to perform a time-dependent measurement. Coincident γ rays were detected at forward angles by the ORGAM [13], and backward angles by the MINIBALL [14] arrays. The charge-state distributions of ^{56}Fe ions traversing nickel foils at various energies were measured at the Australian National University (ANU) Heavy Ion Accelerator Facility (HIAF) [15].

2.2 Hyperfine interaction in ions recoiling in vacuum

The RIV technique can be used to measure the nuclear g factor via a perturbation of the γ-particle angular correlation arising from the nuclear-electronic dipole interaction [3]. When ions recoil in vacuum the electron spins (J) are presumed to have no preferred orientation in space, whereas the nuclear spins (I) have been oriented by the Coulomb excitation. The nuclear and electron spins then couple and, in the vector model picture, begin to precess about their total spin (F) at a frequency proportional to the g factor. This interaction is illustrated in Fig. 1. The periodic de-alignment and re-alignment of the nuclear spin perturbs the angular correlation, alternately attenuating and restoring the anisotropy of the angular correlation. The periodic attenuation factor [3] is

$$G_k(t) = \sum_{F,F'} \frac{(2F+1)(2F'+1)}{2J+1} \begin{Bmatrix} F & F' & k \\ I & I & J \end{Bmatrix}^2 e^{i\omega_{FF'}t}, \quad (1)$$

where t is time, the quantum spin numbers have their established designation, the curly braces signify a Wigner 6-J symbol, and the precession frequency is

$$\omega_{FF'} = \frac{gB_{HF}}{2J}\frac{\mu_N}{\hbar}[F(F+1) - F'(F'+1)], \quad (2)$$

where B_{HF} is the hyperfine-field strength (which can be calculated from atomic theory), and μ_N is the nuclear magneton. Note that $w_{FF'}$ varies for each F, F' coupling, resulting in a superposition of different frequencies when $J > 1/2$.

When multiple atomic states contribute in sequence, their effect is multiplicative. Alignment lost through precession of a prior state is never regained. The attenuation coefficient resulting from atomic decays through a sequence of states is thus

$$G_k^A(t_N) = G_k^1(t_1)\prod_{i=2}^{N} G_k^{(i)}(t_i - t_{i-1}), \quad (3)$$

where $G_k^{(i)}$ is the attenuation coefficient in state i, t_i is the time at which the state decayed, and N is the total number of states in the decay cascade up to time t_N.

Generally, there will be a distribution of charge states (ionic species), each contributing a large number of atomic decay cascades. The average contribution of G_k^A for each ionic species must be considered. Accounting for this, the experimentally measured value is determined by

$$\bar{G}_k(t) = \sum_{Q}^{N_Q} c_Q \sum_{A}^{N_A} G_k^{AQ}(t)/N_A, \quad (4)$$

where A represents an atomic-decay chain, N_A is the number of atomic-decay chains in an individual ionic species, Q, N_Q is the number of species, and c_Q is the fractional population of an individual ionic species.

2.3 Atomic structure calculations

To model the hyperfine interaction the atomic structure information of the ionic species must be obtained. Progress in the field of atomic physics allows the calculation of atomic wavefunctions with great accuracy. One particular solution for calculating atomic properties, the General Relativistic Atomic Structure Package (GRASP), is freely available under the MIT license [16]. The GRASP numerically solves the multiconfiguration Dirac-Hartree-Fock equations for atomic-state functions (ASFs) to obtain radial wavefunctions. The vital point in using the GRASP is understanding how the ASF is constructed. This is done using a linear combination of individual configuration-state functions (CSFs), calculated by

$$\Psi(\gamma PJ) = \sum_{i=1}^{N} c_i \Phi(\gamma_i PJ), \quad (5)$$

where N is the number of chosen CSFs, with each CSF i having a mixing coefficient c_i, and a Slater determinant Φ defined by the electron configuration γ_i, parity P and angular momentum J.

From Eq. (5) it can be seen that all CSFs having the same parity and angular momentum can contribute to a given ASF. To obtain the most accurate solution one would include every CSF having shared P and J up to the continuum states. However, this is impractical as convergence becomes more difficult and computation time becomes exponentially longer as the number of CSFs increases. As such, when performing these calculations, one should choose CSFs that mix significantly with the ASF. Because we aim to simulate spectral cascades the approach taken has been to calculate ASFs for only valence configurations. The CSFs chosen for these calculations allowed for single and double excitations from the principal quantum number $n = 2$ electrons to improve transition-rate calculations, and a single excitation from the $n = 1$ electrons to improve the hyperfine-interaction calculation. ASFs and CSFs were taken up to a value of n where the number of CSFs exceeded $\sim 10^6$, at which point computation time was already quite long ($\sim$ 1 week). This generally took the highest-energy ASF up to the ionisation energy, otherwise the list was resticted to energy levels below 1000 eV. Once solutions are obtained, the calculated energy levels were compared to those in the US National Institute of Standards and Technology database for atomic spectra (https://www.nist.gov/pml/atomic-spectra-database), and found to agree better than 1% in all cases, and 0.1% in most. This comparison is helpful in determining whether the radial wavefunctions have converged on an accurate solution. Another way convergence was assessed was to compare the results of the two oscillator strength calculation approaches (alternate forms for the dipole operator, or gauges) the GRASP takes, namely the length and velocity forms [17]. Disagreement indicates the solution is not self-consistent. Most were found to agree better than 1%, with poor agreement only observed for slow transitions between high-energy states, which were deemed unimportant in the present context due to the unlikeliness of their population or observation.

2.4 Monte-Carlo simulation

Finding an exact mathematical solution to the complex problem of calculating $\bar{G}_k(t)$ is not practical. Instead, the Monte-Carlo method is used to obtain a solution by conducting a "virtual experiment" using the atomic structure calculations. For a given species an initial atomic state is selected at random following the chosen energy distribution (e.g. Boltzmann or uniform). A nuclear survival time for the event is then generated by

$$t_N(\tau_N) = -\log_e(P) \times \tau_N, \quad (6)$$

where τ_N is the nuclear state lifetime, and P is a random number evenly distributed between $(0, 1]$. Then, the following procedure is iterated (after initialising the cumulative atomic survival time t_c to zero) :

1. If the atomic lifetime τ_a is finite, generate an atomic survival time (t_a) for the atomic state as per Eq. (6), but with τ_a in place of τ_N. Otherwise, set t_a to the nuclear survival time (t_n) minus t_c ($t_a = t_n - t_c$) and end the event.
2. If the cumulative and atomic survival time exceed the nuclear survival time ($t_c + t_a > t_n$) then set $t_a = t_n - t_c$ and end the event. Otherwise, add t_a to t_c.
3. Select a new atomic state based on the transition probabilities.

Atomic levels and t_a values are recorded for each iteration. This procedure produces an event consisting of a number of atomic-level references and survival times, with a cumulative atomic survival time equal to the nuclear survival time. This information is then used to evaluate the atomic-state population through time, and once that is performed for each ionic species, to calculate $\bar{G}_k(t)$.

2.5 Attenuation of γ-particle angular correlations

The perturbed γ-ray angular distributions from oriented nuclei can be used to perform g-factor measurements [18]. When an excited 2^+ state is populated via Coulomb excitation the statistical tensor defining the orientation of the state can be calculated from semi-classical electromagnetic theory [19]. It is determined largely by the experimental particle-detection geometry with little sensitivity to the $E2$ matrix elements. The angular correlation [20] can be calculated by

$$W(t, \phi, \theta) = \sum_{k,q} \sqrt{2k+1}\rho_{kq} G_k(t) F_k Q_k D^{k*}_{q0}(\phi, \theta, 0), \quad (7)$$

where $k = 0, 2, 4$ and $-k \leq q \leq k$, ρ_{qk} is the statistical tensor defining the spin alignment of the excited nuclear state, $G_k(t)$ is the attenuation coefficient, F_k represents the F-coefficients for the γ-ray transition [19], Q_k is the attenuation factor due to the finite γ-ray detector size, and D^k_{q0} is the Wigner D rotation matrix [19]. The angles ϕ and θ are spherical polar coordinates, where the position of the beam spot on the target represents the origin, and the beam direction defines the z axis. ϕ is the relative azimuthal angle between the γ-ray detector and the particle detector, and θ is the polar angle of the γ-ray detector.

The time-dependent attenuation coefficient, $G_k(t)$, can be measured using a plunger device, which quenches the hyperfine interaction at a particular distance (i.e after a set flight time) by implantation into a foil [21]. By measuring γ-particle coincidence events using a segmented, annular particle detector, θ- and ϕ-dependent angular correlations can be measured as a function of time. $G_k(t)$ values can be obtained by fitting Eq. (7) to the data, with G_k ($k = 2, 4$) as free parameters ($G_0 = 1$). The G_k values can also be calculated *a priori* with the g factor the only unknown parameter. Atomic states having spin $J = 1/2$ are best suited to measure g factors as they have a single cosine frequency over the summation of F, F'. In our case Na-like ions, having $J = 1/2$ ground states, are the most useful ionic species to populate.

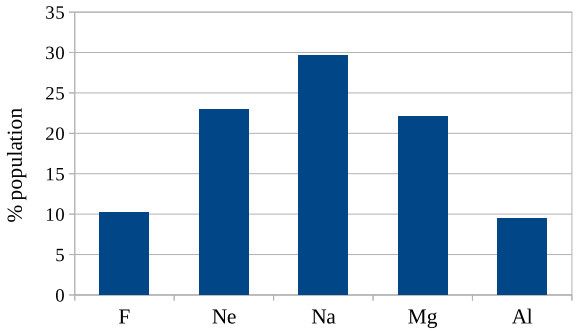

Figure 2. Estimated charge-state distribution of ^{56}Fe ions in the TDRIV measurement at ALTO.

3 Results and Discussion

3.1 Charge-state distribution

Figure 2 shows the expected charge-state distribution of ^{56}Fe ions in the ALTO measurement, centred on Na-like ions. The distribution is quite broad, with the neighbouring Ne- and Mg-like species each comprising $\sim 70\%$ of the population of the Na-like. The Ne-like ground state will be dominantly occupied due to the closed electron shell and, having $J = 0$, there will be no net hyperfine interaction. The effect will be to reduce the amplitude of the Na-like $J = 1/2$ frequency in the average attenuation coefficient $\bar{G}_k(t)$. The Mg-like species will have many populated excited atomic states, close in energy, due to having two valence electrons. The hyperfine interaction in such species appears as a quasi-exponential attenuation through time, again effectively reducing the Na-like frequency amplitude. The effect is the same for the Al-like charge state. The single-hole F-like ions have low-energy, long-lived atomic states with hyperfine-field strengths similar to the Na-like atomic states. If they are strongly populated, the resulting interference patterns may be difficult to deconvolute.

3.2 Atomic-state populations

Atomic energy levels and transition rates together with the Monte Carlo calculation were used to explore the ways in which the population of atomic states could vary through time. These populations obviously depend on the initial distribution of atomic states, which is not well known. A comparison of the atomic population distributions for Na-like ^{56}Fe ions with time, one having an initial population with a Boltzmann energy distribution of mean energy $T = 100$ eV, and the other a uniform distribution up to the highest-energy ASF, is shown in Fig. 3. Both initial distributions populate similar atomic states at longer times (> 25 ps), but have different relative intensities on the order of the nuclear lifetime (10 ps). The initial Boltzmann distribution results in low-energy states being preferentially populated from early time points, with the ground state having a dominant contribution from $t = 0$. Feeding cascades from higher-energy states are also much less influential.

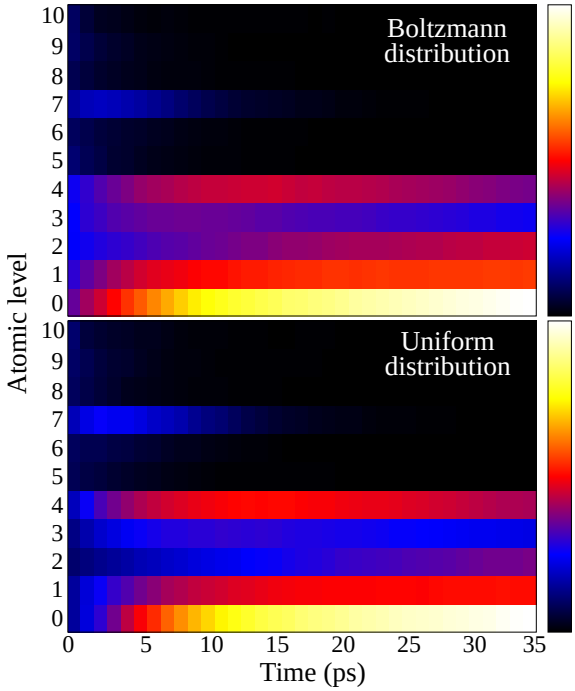

Figure 3. Na-like atomic-state distributions for Fe ions, showing an initial Boltzmann ($T = 100$ eV) vs uniform distribution (all calculated ASFs). The y axis shows the energy-ordered level index. The temperature scale is set relative to the most intense population on the plot. Higher-excited states, which feed the lower states in the initial few picoseconds, are included in these calculations, but are not shown.

Of the five charge states present, only two have atomic states with observable frequencies, these being the Na-like and F-like charge states. Fig. 3 shows that, irrespective of whether a Boltzmann or uniform initial distribution is chosen, three low-lying Na-like atomic states, $3s_{1/2}$ (0), $3p_{1/2}$ (1) and $3d_{5/2}$ (4), where the numbers in parentheses are the state labels in Fig. 3, are rapidly (< 5 ps) populated. Of these three, only the $3s_{1/2}$ and $3p_{1/2}$ states have observable frequencies. In F-like ions, proximity to the neon shell-gap results in the ground and first-excited state ($2p_{3/2}$ and $2p_{1/2}$ holes) being almost solely populated within a few picoseconds, and both have observable frequencies. The pure G_k vs t plots for these four frequencies are shown in Fig. 4.

3.3 Fitting the g factor

Measured $G_k(t)$ values were obtained by fitting Eq. (7) to the data as described in Sec. 2.5. For clarity of analysis, a subset of the total data was chosen. This subset was taken by the ORGAM detectors (having high statistics) and rejected γ-rays emitted by nuclei which had decayed in flight, selecting for $G_k(t)$. By varying the g factor used in the calculation of $\bar{G}_k(t)$ from the Monte-Carlo simulation events, an optimal fit to the data points can be found. However, another important parameter is the initial distribution of atomic states, as this will affect the population strength of the observable frequencies and the aver-

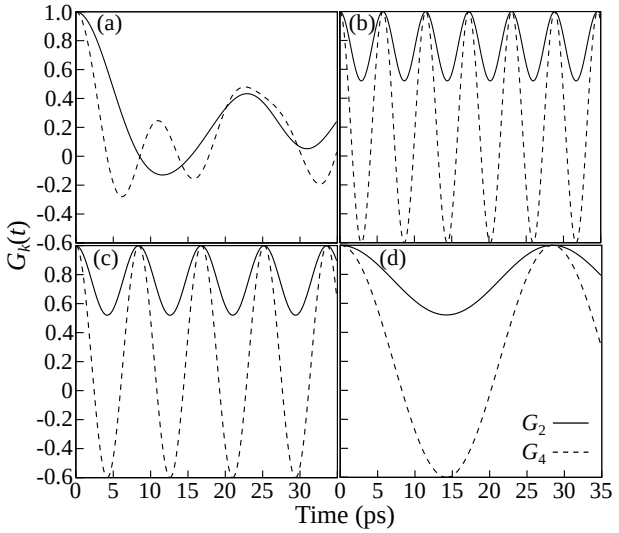

Figure 4. Individual $G_k(t)$ plots for Fe ion (a) F-like $2p_{3/2}$, (b) F-like $2p_{1/2}$, (c) Na-like $3s_{1/2}$, and (d) Na-like $3p_{1/2}$. These are all evaluated with $g(2_1^+; \mathrm{Fe}^{56}) = 0.51$, as previously reported [22].

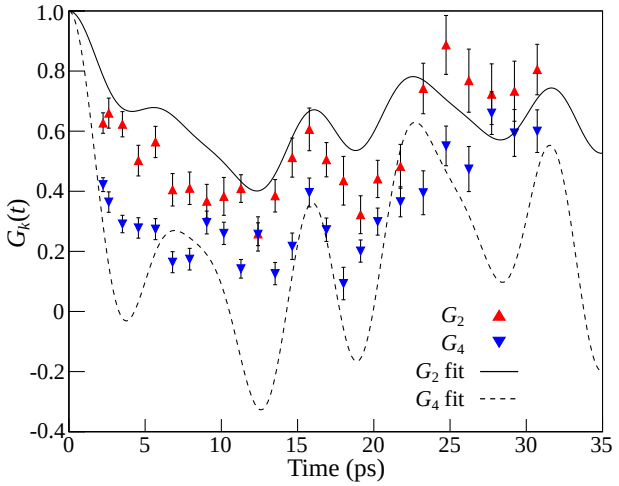

Figure 5. Experimental $G_k(t)$ values obtained by free-fitting measured angular correlations, and a superposition of the frequencies shown in Fig. 4 having relative populations 25% (a), 15% (b), 35% (c) and 25 % (d), and $g = 0.55$, producing an optimal fit the period peak at 16 ps.

age magnitude of the $\bar{G}_k$ values. It is illuminating to consider, individually, the major contributing atomic states, and whether they have precession frequencies that will appreciably affect the measurement. The atomic-state-population heatmaps (Fig. 3) can help guide reasonable proportions in which to mix the frequencies. A frequency superposition of the major contributing states allows grand features of the measured $G_k(t)$ values to be probed. If these features of the G_k vs t plot can be unambiguously reproduced, then the g factor can be robustly determined.

The measured $G_k(t)$ values are shown in Fig. 5 along with a fit using only the frequencies shown in Fig. 4. Focusing on the experimental data points, there are two notable features: the peak-like increase in G_k at 16 ps, and the broader increase at 25 ps. By reference to Fig. 4, the interference pattern between F-like $2p_{1/2}$ and Na-like $3s_{1/2}$ produces a constructive peak at 16 ps, but interferes more destructively elsewhere. This near-cancellation can explain the smoother variation from 6 to 10 ps, and 23 to 27 ps. Both F-like $2p_{3/2}$ and Na-like $3p_{1/2}$ can contribute to the increase in G_k at 25 ps, but Na-like $3p_{1/2}$ appears to be dominant. Additionally, the different effective frequencies for G_2 and G_4 from F-like $2p_{3/2}$, resulting from its $J = 3/2$ atomic spin, can explain the proximity of G_2 and G_4 values near 10 ps and 20 ps. The frequency superposition in Fig. 5 was made to be in line with the measured charge state distribution and predicted atomic-state populations, and to reproduce the peaks at 16 ps and at 25 ps; this gives $g \approx 0.55$. Changing g by more than ± 0.02 causes significant misalignment of the fit from these prominent features.

When attempting to fit the entire timespan, the data seem to show a changing population of states through time. Initially, a strong contribution from the F-like states can match the initial decrease, with the $2p_{3/2}$ state responsible for the proximity of G_2 and G_4 around 10 ps. After this point, increasing population of the Na-like states can match the sharp peak at 16 ps, and their continued population increase can bring about the large peak at 25 ps. A plausible explanation is that higher-energy excited atomic states are strongly populated in the Na-like ions initially, and then decay to the low-energy states, with the initial distribution perhaps being approximately Gaussian. This hypothesis is currently under investigation. The complicated superposition of changing populations makes a global fit difficult. Preliminary results from a global fit indicate that the g factor could possibly be determined with an uncertainty below ± 0.01. It should be noted that systematic sources of uncertainty are yet to be quantified, with the most significant expected to be the uncertainty in the absolute time offset (plunger zero-distance). However, even at this stage of analysis, fitting of major trends can evidently provide a robust measure of the g factor.

It should be clarified that the G_k values are highly correlated, so free-fitting by χ^2 minimisation may not give correct relative magnitudes of G_2 and G_4. It will, however, reveal frequency trends that are useful in guiding the data analysis. As such, discrepancies in the magnitude of the fitted vs measured values should not be considered too harshly at this preliminary stage. An approach by which G_k values are calculated *a priori* and fitted directly to the angular correlation, while also allowing atomic-state populations to vary in time realistically, is in progress.

4 Conclusion

The time-dependent RIV measurement technique has been demonstrated as a promising way to measure $g(2_1^+)$ values in short-lived nuclear states of radionuclides. Detailed Monte-Carlo simulations based on atomic-structure calculations reveal that multiple atomic states contribute to the hyperfine interaction for nuclei around $Z = 30$, creating a superposition of frequencies. By modelling and fitting the population of states through time, it appears that the

g factor can be reliably determined. The relevant hyperfine interaction frequencies from a TDRIV data set on ^{56}Fe were identified and suggest $g \approx 0.55$, with an accuracy of $\sim 4\%$. An improved data analysis technique is being developed, from which preliminary results indicate that the g factor could be determined with close to 1% precision, the final precision likely dependent on systematic uncertainties associated with the plunger technique as much as the modelling of the hyperfine fields.

Acknowledgements

The authors are grateful to the academic and technical staff of the IPN ALTO facility and the ANU HIAF for their assistance and maintenance of the facilities. In particular, the authors would like to thank J. Ljungvall, I. Matea, T. Konstatinopoulos, K. Gladnishki, A. Gottardo and D. Yordanov for their assistance with the data collection. This research was supported in part by the Australian Research Council under grant number DP170101673. A.G. acknowledges the support of the P2IO Excellence Laboratory. B.P.M. acknowledges the support of the Australian Government Research Training Program. Support for the ANU Heavy Ion Accelerator Facility operations through the Australian National Collaborative Research Infrastructure Strategy (NCRIS) program is acknowledged.

References

[1] N. Benczer-Koller, G.J. Kumbartzki, Journal of Physics G: Nuclear and Particle Physics **34**, R321 (2007)

[2] A.E. Stuchbery, Hyperfine Interactions **220**, 29 (2013)

[3] G. Goldring, in *Heavy Ion Collisions*, edited by R. Bock (North-Holland Pub. Co., 1982), Vol. 3, p. 483

[4] N.J. Stone, A.E. Stuchbery, M. Danchev, J. Pavan, C.L. Timlin, C. Baktash, C. Barton, J.R. Beene, N. Benczer-Koller, C.R. Bingham et al., Phys. Rev. Lett. **94**, 192501 (2005)

[5] J.M. Allmond, A.E. Stuchbery, D.C. Radford, A. Galindo-Uribarri, N.J. Stone, C. Baktash, J.C. Batchelder, C.R. Bingham, M. Danchev, C.J. Gross et al., Phys. Rev. C **87**, 054325 (2013)

[6] A.E. Stuchbery, J.M. Allmond, A. Galindo-Uribarri, E. Padilla-Rodal, D.C. Radford, N.J. Stone, J.C. Batchelder, J.R. Beene, N. Benczer-Koller, C.R. Bingham et al., Phys. Rev. C **88**, 051304(R) (2013)

[7] A.E. Stuchbery, J.M. Allmond, M. Danchev, C. Baktash, C.R. Bingham, A. Galindo-Uribarri, D.C. Radford, N.J. Stone, C.H. Yu, Phys. Rev. C **96**, 014321 (2017)

[8] A. Kusoglu, A.E. Stuchbery, G. Georgiev, B.A. Brown, A. Goasduff, L. Atanasova, D.L. Balabanski, M. Bostan, M. Danchev, P. Detistov et al., Phys. Rev. Lett. **114**, 062501 (2015)

[9] A.E. Stuchbery, N.J. Stone, Phys. Rev. C **76**, 034307 (2007)

[10] N.J. Stone, J.R. Stone, P. Jönsson, Hyperfine Interactions **197**, 29 (2010)

[11] X. Chen, D.G. Sarantites, W. Reviol, J. Snyder, Phys. Rev. C **87**, 044305 (2013)

[12] J. Ljungvall, G. Georgiev, S. Cabaret, N. Karkour, D. Linget, G. Sedes, R. Chevrier, I. Matea, M. Niikura, M.D. Salsac et al., Nucl. Inst. Meth. A **679**, 61 (2012)

[13] C.L. Galliard, Tech. rep., IPN Orsay, IPN Orsay, University of South Paris, Orsay, France (2019), `http://ipnwww.in2p3.fr/Orgam?lang=en`

[14] N. Warr, J. Eberth, G. Pascovici, H.G. Thomas, D. Weißhaar, D. Habs, P. Reiter, P. Thirolf, D. Schwalm, C. Gund et al., *MINIBALL: A Gamma-ray spectrometer for exotic beams* (2003), pp. 490–496

[15] A.E. Stuchbery, A.B. Harding, D.C. Weisser, N.R. Lobanov, Nuclear Instruments and Methods in Physics Research Section A: Accelerators, Spectrometers, Detectors and Associated Equipment **951**, 162985 (2020)

[16] C.F. Fischer, G. Gaigalas, P. Jönsson, J. Bieroń, Computer Physics Communications **237**, 184 (2019)

[17] C.F. Fischer, T. Brage, P. Jönsson, *Computational Atomic Structure: An MCHF Approach* (Institute of Physics Publishing Bristol and Philadelphia, 1997)

[18] A.E. Stuchbery, M.P. Robinson, Nucl. Instrum. Meth. Phys. Res. A **485**, 753 (2002)

[19] K. Alder, A. Winther, *Electromagnetic excitation: theory of Coulomb excitation with heavy ions* (Amsterdam: North Holland, 1975)

[20] A.E. Stuchbery, Nuclear Physics A **723**, 69 (2003)

[21] A. Kusoglu, A.E. Stuchbery, G. Georgiev, A. Goasduff, L. Atanasova, D.L. Balabanski, M. Bostan, M. Danchev, P. Detistov, K. Gladnishki et al., J. Phys. C **590**, 012041 (2015)

[22] M.C. East, A.E. Stuchbery, S.K. Chamoli, A.N. Wilson, H.L. Crawford, J.S. Pinter, T. Kibédi, P.F. Mantica, Phys. Rev. C **79**, 024303 (2009)